J Neurosurg 90:160–168, 1999

Accuracy of true frameless stereotaxy: in vivo measurement and laboratory phantom studies

Technical note

NEIL L. DORWARD, F.R.C.S., OLAF ALBERTI, M.D., JAMES D. PALMER, F.R.C.S.(SN), NEIL D. KITCHEN, F.R.C.S.(SN), AND DAVID G. T. THOMAS, F.R.C.P., F.R.C.S.(ED)

University Department of Neurosurgery, Institute of Neurology, National Hospital for Neurology and Neurosurgery, London, United Kingdom

The authors present the results of accuracy measurements, obtained in both laboratory phantom studies and an in vivo assessment, for a technique of frameless stereotaxy. An instrument holder was developed to facilitate stereotactic guidance and enable introduction of frameless methods to traditional frame-based procedures. The accuracy of frameless stereotaxy was assessed for images acquired using 0.5-tesla or 1.5-tesla magnetic resonance (MR) imaging or 2-mm axial, 3-mm axial, or 3-mm helical computerized tomography (CT) scanning. A clinical series is reported in which biopsy samples were obtained using a frameless stereotactic procedure, and the accuracy of these procedures was assessed using postoperative MR images and image fusion.

The overall mean error of phantom frameless stereotaxy was found to be 1.3 mm (standard deviation [SD] 0.6 mm). The mean error for CT-directed frameless stereotaxy was 1.1 mm (SD 0.5 mm) and that for MR image–directed procedures was 1.4 mm (SD 0.7 mm). The CT-guided frameless stereotaxy was significantly more accurate than MR image–directed stereotaxy ($p = 0.0001$). In addition, 2-mm axial CT-guided stereotaxy was significantly more accurate than 3-mm axial CT-guided stereotaxy ($p = 0.025$). In the clinical series of 21 frameless stereotactically obtained biopsies, all specimens yielded the appropriate diagnosis and no complications ensued. Early postoperative MR images were obtained in 16 of these cases and displacement of the biopsy site from the intraoperative target was determined by fusion of pre- and postoperative image data sets. The mean in vivo linear error of frameless stereotactic biopsy sampling was 2.3 mm (SD 1.9 mm). The mean in vivo Euclidean error was 4.8 mm (SD 2 mm). The implications of these accuracy measurements and of error in stereotaxy are discussed.

KEY WORDS • frameless stereotaxis • computer-assisted surgery • neuronavigation • stereotactic biopsy • in vivo accuracy

CONTEMPORARY imaging of individual neuroanatomy has achieved such exquisite detail that mental transposition of imaging information to a surgical field necessarily loses much of this information. Neuronavigation has successfully overcome this difficulty; considerable experience has now accrued with image guidance systems,[10,13,14,23,25,28] and there is increasing evidence of their clinical benefit.[2,7,15,18,26,28] In contrast with its use in open neurosurgical operations, image guidance has had little impact on the traditional frame-based stereotactic biopsy procedures, depth electrode insertion, and functional neurosurgery. Neuronavigation has the potential to dissociate image acquisition from surgery, provide interactive target selection, and increase the therapeutic options without restriction of surgical access or the need for magnetic resonance (MR) imaging–compatible stereotactic equipment.

To be truly stereotactic, frameless methods must provide precise guidance of delicate instruments to a preselected discrete target at any site within the cranium, without deviation or collateral brain injury. Although image guidance of a tracked instrument can be achieved relatively simply,[3,17,27] hand-held devices cannot satisfy the requirements of stereotaxy. Therefore, for frameless stereotaxy to be achieved, an instrument guide is required. This should reach all parts of the cranial vault, lock in place rigidly to provide robust support, allow fine correction of trajectory settings, adapt to a variety of instruments, and be compatible with image guidance tracking. Although attempts to adapt traditional neurosurgical devices to this task have been reported,[11] none has been entirely successful because of the devices' excessive movement, inflexibility, or obstruction of the surgical field. In addition, for frameless stereotaxy to be accepted,

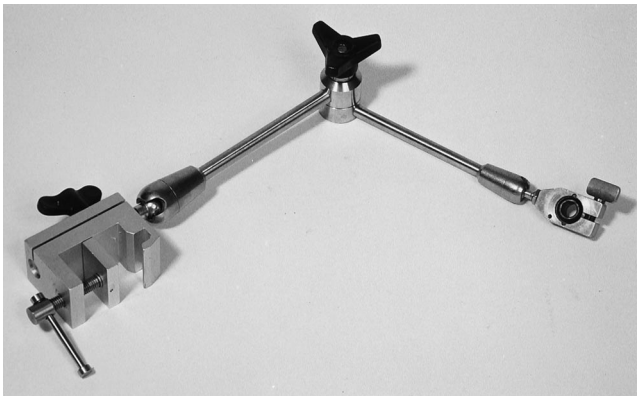

FIG. 1. Photograph showing the adjustable, locking, adaptable instrument holder. The proximal block attaches to the Mayfield head clamp and the arm is locked in position with the central handle. The distal trapped ball enables fine adjustment of the trajectory and is fixed in position for biopsy retrieval.

the phantom accuracy, diagnostic yield, and complication rate must be comparable with those procedures that involve contemporary stereotactic frames.

In this paper we describe an instrument holder developed to achieve frameless stereotaxy and present the results of laboratory phantom accuracy studies of this technique and a clinical series in which biopsy specimens were obtained using frameless stereotaxy, and we describe an in vivo accuracy study of the same technique. The contributions of frameless stereotactic methods and the implications of errors in stereotaxy are discussed.

Description of Equipment

Neuronavigation System

The neuronavigation system used throughout this study was the EasyGuide Neuro system (Philips Medical Systems Nederland BV, Best, The Netherlands). The components of this device include a variety of hand-held pointers fitted with infrared light-emitting diodes, a pair of cameras in a table-mounted array, and a mobile computer workstation. The position of a pointer is continuously displayed on the computer monitor as the intersection of standard orthogonal (axial, coronal, and sagittal) planes obtained from preoperative images. An additional screen area displays either a perpendicular or in-line pointer view. Software packages installed in the system include path planning, electronic callipers, and pointer elongation tools. A complementary radiology workstation (CT/MR EasyVision; Philips Medical Systems Nederland BV) was used for image fusion.

Frameless Stereotaxy Instrument Guide

A stereotactic guide was developed[8] that would adapt to a variety of instruments, was freely adjustable to reach all parts of the cranium, would lock in place rigidly, and would allow fine correction of the trajectory setting (Fig. 1). The mounting block enabled fixation to a Mayfield clamp (OMI Surgical Products, Cincinnati, OH), and the three joints locked simultaneously without producing torsional movement. The trapped ball contained a large central channel to accept instrument-holding blocks with inner bores of 2- to 5.25-mm caliber, allowing for guidance of a wide variety of instruments (Fig. 2). A dedicated block for use with navigation system pointers was produced with an incomplete inner bore that placed the pointer tip at the geometric center of the trapped ball.

Technique of Frameless Stereotaxy

The method developed for frameless stereotaxy was composed of five stages: 1) image acquisition; 2) image-to-patient registration; 3) entry point selection; 4) target and trajectory definition; and 5) biopsy retrieval.

Self-adhesive fiducial markers were attached to the patient's scalp in a standard pattern prior to imaging. The marker positions were: midforehead, glabella, both temples, vertex, both mastoids, and both parietal eminences. An additional two to four fiducial markers were applied in a cluster over the region of interest. The images acquired were either gadolinium-enhanced MR images (0.5-tesla Vectra or 1.5-tesla Signa imaging systems; General Electric, Milwaukee, WI) or contrast-enhanced computerized tomography (CT) scans (Somatom 4 scanner; Siemens Corp., Erlangen, Germany). For the Signa MR im-

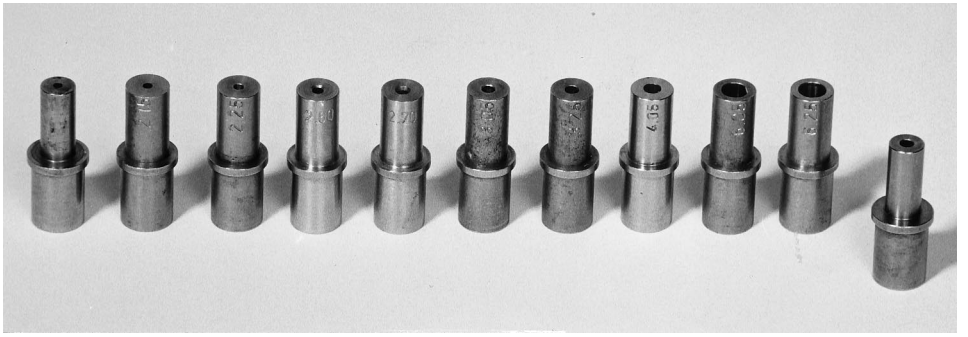

FIG. 2. Photograph showing a selection of the instrument-holding blocks that fit into the distal trapped ball. Each has a central channel of specific diameter to provide guidance for a particular instrument. The blocks demonstrated here have inner bores ranging in caliber from 2 to 5.25 mm, which correspond to the outer diameters of some widely used biopsy instruments, aspiration needles, recording electrodes, and endoscopes.

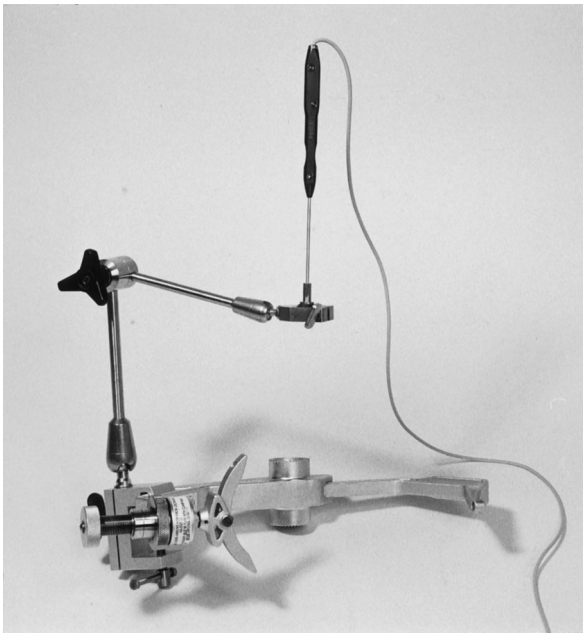

FIG. 3. Photograph showing the instrument holder mounted on the Mayfield head clamp and locked in position. A pointer is seen docked in the pointer block, located in the trapped ball. Fine adjustment of pointer trajectory and length of virtual elongation enables interactive target selection.

aging system, the protocol was a spin-echo gradient sequence with minimum repeat and echo times, a 50˚ flip angle, 256 × 256–cm matrix, 24-cm field of view (FOV), and a 1.5-mm slice thickness. The imaging protocol for the Vectra MR imaging system was a 42-msec repeat time, 15-msec echo time, 50˚ flip angle, 192 × 256–cm matrix, 24-cm FOV, and a 2-mm slice thickness. For sequential axial CT scans, there was a 512 × 512–cm matrix, 23-cm FOV, 0˚ gantry tilt, and the sliced thickness was either 2 mm with a 2-mm slice separation or 3 mm with a 3-mm slice separation. The parameters for helical CT scans were: a 512 × 512–cm matrix, 20.5-cm FOV, 0˚ gantry tilt, and a 3-mm slice thickness. The resultant voxel dimensions for the Signa MR images were x = 0.93 mm, y = 0.93 mm, and z = 1.5 mm and those for the Vectra MR images were x = 1.25 mm, y = 0.93 mm, and z = 2 mm. For sequential axial CT images the voxel dimensions were x = 0.45 mm, y = 0.45 mm, and z = 2 or 3 mm. The voxel dimensions for helical CT images were x = 0.4 mm, y = 0.4 mm, and z = 3 mm. The mean intervoxel distance (MID) was calculated for each study from these values as the mean of the sum of distances from the center of a voxel to the center of all adjacent voxels. In these volumetric data sets, each voxel was adjacent to 26 others and the MID was calculated simply from the known voxel dimensions of that study, thus:

$$\text{MID} = [2x + 2y + 4(\sqrt{x^2 + y^2}) + 2z + 4(\sqrt{x^2 + z^2}) + 4(\sqrt{y^2 + {}^2}) + 4(\sqrt{x^2 + y^2 + z^2})]/26$$

Image-to-patient registration was performed using a fiducial marker–based method. The patient was placed in position and a Mayfield head clamp was applied; the location of each fiducial marker was identified on the preoperative images, and a hand-held pointer was used to define the position of each marker on the head. The system matched the image and patient fiducial positions and derived the root mean square error (RMSE) of registration. The error associated with each fiducial marker was determined; those with an unacceptable discrepancy were deleted and reregistration was performed.

Entry points were selected either from positions that had been predefined on the images with path planning or by using a hand-held pointer for interactive planning. In the latter situation, virtual pointer elongation displayed structures along the pointer trajectory from surface to target. As the pointer tip position was altered, the trajectory was displayed in the images in near-real time. An appropriate entry site was selected, the area was prepared for surgery, and a burr hole was constructed. The instrument guide was clamped to the vertical portion of the Mayfield head clamp and locked in position with the trapped ball over the burr hole. A pointer was inserted into the trapped ball (Fig. 3) and virtual elongation was used to display the trajectory and target. Fine adjustment of both the trapped ball position and the length of virtual elongation was used to define the optimum target site. The trapped ball was locked in position, and the pointer block was exchanged for the appropriate instrument-guide block. The target position in the orthogonal image reformats was captured and stored in the workstation's memory. Biopsy retrieval was performed using a standard Sedan–Nashold side cutting needle (Radionics Inc., Burlington, MA) with a 2-mm outer diameter and a 10-mm side window. The depth to the target was calculated from the length of virtual elongation used (displayed automatically by the system) plus 28 mm (the distance below the top of the block to which the pointer tip passed). A stop was placed on the biopsy needle at the calculated distance from the center of the side window. Thus, the target would be expected to lie at the center of the biopsy core. The needle was guided to the target by the instrument block and specimens were retrieved from each quadrant.

Following each surgical procedure, the arm was tested for movement occurring during biopsy retrieval. The biopsy needle was removed, the instrument block was exchanged for the pointer block, and the pointer was replaced in the trapped ball. The same length of virtual extension was applied and the check target was captured. The coordinates (image data set x, y, and z values) of these check targets were later compared with those for the respective biopsy target and any difference was calculated.

Laboratory Phantom Accuracy Experiments

The phantom was a molded plastic skull mounted on a Perspex base that was compatible with both CT and MR imaging. Standard self-adhesive fiducial markers were attached to the outer surface of the skull in positions used clinically, and the phantom was imaged according to clinical protocols. Within the skull were Perspex shapes; 20 image-localizer bone screws (Leibinger, Tütlingen, Germany) were inserted into these and spread throughout the skull volume in every orientation. A cup attachment was screwed onto the top of each of these localizers to mount interchangeable imaging and position markers. The imaging attachments were composed of plastic spheres on

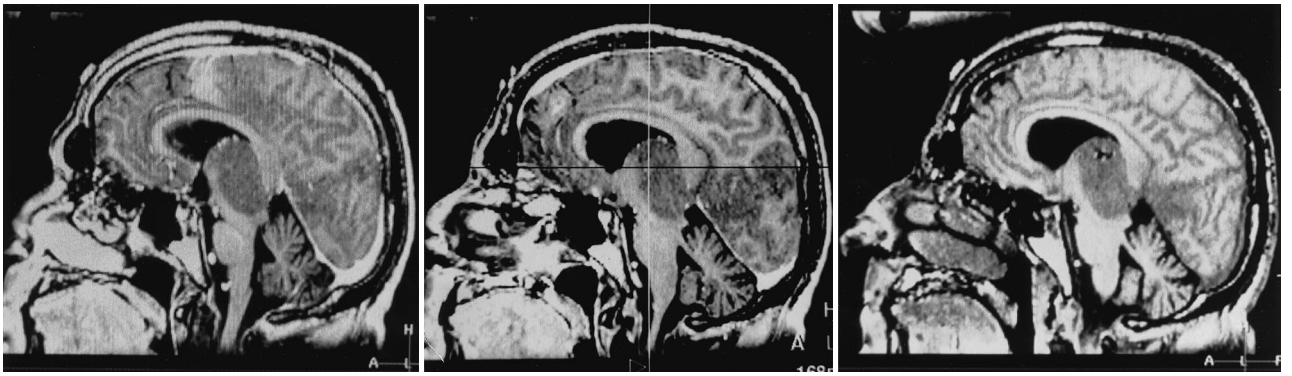

FIG. 4. Case 5. Sagittal MR images selected from the series of frameless stereotactic biopsy procedures demonstrating the preoperative appearance of the lesion *(left)*, the captured intraoperative target *(center)*, and the postoperative appearance of the biopsy site *(right)*. Fusion of preoperative and postoperative data sets enabled the in vivo error to be calculated.

a stalk with a central metal ball for CT imaging or a hollow core for MR imaging solutions. The position markers were flat caps with a central dimple. These attachments were manufactured in such a manner that the position of the central dimple of the position marker cap corresponded precisely with the center of the imaging spheres.

The phantom was mounted on the operating table in a Mayfield clamp, the camera array was attached in the usual position, and fiducial marker–based registration was performed. Each imaging marker was selected in turn as the target for frameless stereotaxy and localized using a technique that reproduced the clinical procedure. Thus, the entry point was selected with the pointer and the arm locked in position, virtual elongation was adjusted to identify the target, and the trajectory was finely altered with the trapped ball. Once the instrument holder was placed in position, the depth to the target was calculated, and a depth stop was set on a sharp rigid needle. The pointer block was exchanged for the appropriate needle guide block and the needle was inserted. The distance from the needle tip to the central dimple of the localizer cap was measured with microcallipers. The entire process from fiducial marker definition and registration to error measurement was repeated five times for each MR and CT imaging data set.

In Vivo Accuracy Assessment

In vivo accuracy was determined for a series of frameless stereotactic biopsy procedures. Patients underwent preoperative imaging, which was performed with a Vectra or Signa MR imaging system or a 3-mm axial CT scanner. These preoperative data sets were transferred to the Easy Guide Neuro system and the EasyVision CT/MR workstation. The intraoperative biopsy target (three orthogonal views) was captured in the navigation system database and transferred to the EasyVision CT/MR workstation following surgery. Postoperative volumetric MR imaging was performed within 24 hours of surgery and also transferred to the EasyVision CT/MR workstation. Both pre- and postoperative data sets were registered through manual selection of identical structures. This aligned the coordinate systems of each set of images, allowing the intraoperative target position to be compared with the actual biopsy site position. The biopsy site was clearly identifiable in the postoperative T_1-weighted MR images as a low signal ellipsoid with dimensions similar to the biopsy needle window (Fig. 4). The biopsy site coordinates were taken as the center of the low signal ellipsoid because, during the biopsy procedure, the needle stop was positioned to bring the target to the center of the side window. The difference between the target and the actual biopsy site coordinates was calculated in millimeters, providing the error of localization in linear x, y, and z values. Euclidean errors were calculated from these values according to the formula: $V = (x^2 + y^2 + z^2)$, in which V represents vectorial error.

Statistical Analysis

The results were analyzed for patterns, correlations, and significance as a whole and when segregated according to imaging groups. The statistical tests of significance we used were unpaired two-tailed t tests for normally distributed data and chi-square tests for noncontinuous data (significance established when probability was less than 0.05). Correlations were accepted when the value of the sample correlation coefficient exceeded 0.5 and the associated probability value was less than 0.05. Descriptive statistics are given as the mean and standard deviation (SD) for normally distributed data and as the median with the range for data that is not normally distributed.

Results

Laboratory Phantom Accuracy Experiments

A total of 258 phantom frameless stereotactic procedures were performed (Table 1; Fig. 5) with a mean error of 1.3 mm (SD 0.6 mm). Of the 258 measurements, 120 were CT directed and 138 were MR directed, revealing a mean error for CT-guided phantom frameless stereotaxy of 1.1 mm (SD 0.5 mm) and a mean error for MR-guided phantom frameless stereotaxy of 1.4 mm (SD 0.7 mm). Thus, the accuracy of CT-directed phantom frameless stereotaxy was significantly better than that directed by MR imaging ($p = 0.0001$).

TABLE 1

Summary of the imaging characteristics that determine voxel size and the results of the laboratory phantom measurements of error in frameless stereotaxy

Image Type	Matrix (cm)	FOV (cm)	Voxel Size (mm^3)	MID (mm)	Mean Error (mm)	SD (mm)
0.5-tesla MR	192 × 256	24	2.33	1.65	1.7	0.6
1.5-tesla MR	256 × 256	24	1.30	1.31	1.3	0.6
2-mm axial CT	512 × 512	23	0.41	1.27	1.1	0.5
3-mm axial CT	512 × 512	23	0.61	1.80	1.3	0.6
3-mm helical CT	512 × 512	20.5	0.48	1.78	0.9	0.5

The 120 CT-guided measurements were used in 40 procedures directed by 2-mm sequential axial images, 40 directed by 3-mm sequential axial images, and 40 directed by 3-mm helically acquired images. The mean error for phantom frameless stereotaxy directed by the 2-mm axial CT scans was 1.1 mm (SD 0.5 mm), whereas that for 3-mm axial scans was 1.3 mm (SD 0.6 mm) and that for 3-mm helical scans was 0.9 mm (SD 0.5 mm). Therefore, the narrower cut 2-mm axial CT scans and the 3-mm helical CT scans (with a reduced FOV) were both significantly more accurate than the 3-mm axial CT scan for frameless stereotaxy ($p = 0.025$ and $p = 0.0006$, respectively).

Of the 138 MR image–directed phantom measurements, 95 images were obtained using the 1.5-tesla Signa imager and 43 images using the 0.5-tesla Vectra imager. The mean error for Signa MR image–guided phantom frameless stereotaxy was 1.3 mm (SD 0.6 mm), whereas that for Vectra MR image–guided stereotaxy was 1.7 mm (SD 0.6 mm). Thus frameless stereotaxy performed with Signa images proved to be significantly more accurate than that performed with Vectra MR images ($p = 0.0074$).

In Vivo Accuracy Assessment

A total of 21 frameless stereotactic biopsy procedures were performed in 19 consecutive patients presenting with cerebral mass lesions of unknown origin (Table 2). The patient population was composed of eight women and 11 men from 25 to 76 years of age (median 53 years). The patients' lesions measured between 13.2 mm and 60.5 mm in diameter (median 37 mm) and were located in a variety of cerebral structures. Fiducial marker–based registration required a median of 10 minutes, and the mean registration RMSE was 3.1 mm (SD 0.7 mm), which was achieved with a median of nine fiducial markers (range seven–16). The median duration of the surgical procedure from patient placement on the operating table to reversal of anesthesia was 46 minutes (range 20–105 minutes). The depth of the biopsy target below the locked instrument holder ranged from 40 to 120 mm (median 76 mm). In each case, the final histological diagnosis corroborated that determined from the smear specimen, being high-grade glioma in 17 cases, metastasis in one case, and neurocytoma in one case. There were no intraoperative or postoperative complications. The postoperative target recapture test demonstrated that in no case was there any detectable movement of the instrument holder during biopsy retrieval.

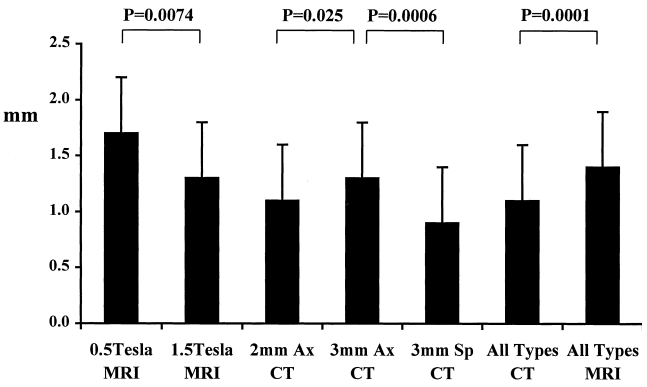

FIG. 5. Bar graph demonstrating the mean error of phantom frameless stereotaxy according to imaging modality. Probability values are given for those imaging methods with significantly different errors. Ax = axial; MRI = MR imaging; Sp = spiral (that is, helical).

Of the 19 patients in this series in whom a biopsy specimen was obtained using the frameless stereotactic procedure, 14 underwent follow-up MR imaging within 24 hours of surgery. Of the 16 biopsy sites in these patients, 15 could be clearly identified in the postoperative images (one cystic lesion precluded comparison, Table 3). Fusion of 13 useful postoperative studies with their corresponding preoperative studies was performed with a mean RMSE of 1.1 mm (SD 0.6 mm). Subtraction of the intraoperative target coordinates from coordinates for the center of the actual biopsy sites revealed a mean linear error of localization of 2.3 mm (SD 1.9 mm). The mean linear error for the nine MR image–directed frameless stereotactic biopsy procedures was 2.6 mm (SD 1.9 mm) and that for the six CT-directed biopsy procedures was 2.5 mm (SD 0.7 mm). When the three linear errors (x, y, and z) were transformed into a vector, the mean error of localization was 4.8 mm (SD 2 mm). The mean euclidean error for the nine MR image–directed biopsies was 4.4 mm (SD 2.1 mm) and that for the six CT-directed biopsies was 5.4 mm (SD 1.5 mm). In these cases there was no correlation between distance to target and error ($r = 0.35$). Separate analysis of the linear error measurements for x, y, and z revealed no statistical difference between them (Table 3). However, the power of analysis was relatively limited because of the small number of cases in each subgroup.

Discussion

Although neuronavigation has become widely accepted as advantageous in open cranial surgery, until recently the technique has had little impact on traditional frame-based stereotactic procedures. The reasons for this include the initial presumption that neuronavigation is intrinsically less accurate than frame-based stereotaxy and the absence of satisfactory instrument guides for frameless stereotaxy. Laboratory investigations have now demonstrated a high degree of accuracy for both optical and arm-based image guidance systems,[12,22,24] and the inadequacies of adapted neurosurgical arms have been overcome by the adjustable, locking, adaptable instrument holder.[8] The resultant method of frameless stereotaxy combines flexibility, simplici-

TABLE 2

*Clinical characteristics of 19 patients in whom a total of 21 frameless stereotactic biopsy samples were obtained**

Case No.	Age (yrs), Sex	Image Type	Site of Lesion	Lesion Size (mm)	No. of FMs	RMSE (mm)	Op Time (hrs)	Target Depth (mm)	Pathological Finding
1	43, F	MR	rt parietal	27.4	11	3.0	1.08	71	metastasis
2	50, M	MR	lt temporal	60.0	7	3.3	0.83	69	glioma
3	56, F	MR	rt parietal	17.0	9	3.2	0.75	75	glioma
4	25, M	MR	rt parietal	26.4	11	3.4	1.75	40	glioma
5	73, M	MR	rt thalamic	42.9	11	3.8	0.83	77	glioma
6	55, M	MR	lt temporal	46.9	10	2.6	1.00	100	glioma
7	53, F	MR	lt frontal	53.3	10	3.1	0.75	72	glioma
8	53, F	MR	lt occipital	54.8	9	2.5	0.70	60	glioma
9	68, F	CT	rt parietal	39.7	16	2.6	0.70	77	glioma
10	57, F	CT	rt parietal	59.0	10	2.5	0.50	77	glioma
11	63, M	CT	Cb peduncle	22.0	9	4.2	0.75	77	glioma
12	70, M	CT	rt frontal	37.8	8	3.1	0.75	78	glioma
		CT	rt frontal	37.8	8	3.1	0.75	82	glioma
13	25, M	MR	lt frontal	60.5	11	3.1	0.58	50	neurocytoma
14	76, M	CT	lt parietal	29.0	8	2.8	0.33	85	glioma
15	38, M	CT	lt parietal	23.6	11	1.9	0.50	55	glioma
16	28, F	MR	lt frontal	13.2	9	2.3	1.00	78	glioma
17	69, F	MR	lt parietal	40.2	9	5.0	0.33	65	glioma
18	57, M	MR	rt thalamic	36.2	8	4.4	0.83	120	glioma
19	53, M	MR	rt temporal	22.6	9	3.0	0.75	88	glioma
		MR	rt temporal	26.7	9	3.0	0.75	103	glioma

* Cb = cerebellar; FMs = fiducial markers.

ty, and unimpeded access to the skull with precise and undeviating instrument guidance. The surgeon may select from virtually infinite entry points, trajectories, and targets while viewing corresponding image reformats. This enables rapid and intuitive selection of the optimum approach to any target.

With the neuronavigation system that we used in this study, registration was performed via a fiducial marker–based rigid body transformation method. Although the accuracy with which registration was achieved was displayed automatically as the RMSE of registration, this should not be confused with the error of point localization. Discrepancies between these arise because the accuracy of registration will seldom be uniform throughout the registered volume. Only if the object were spherical with multiple, evenly distributed fiducial markers, each registered with uniform accuracy, would the RMSE of registration be a good indicator of point accuracy throughout the volume. However, the head is not spherical and has skin of varying mobility, and fiducial markers cannot be evenly distributed around the brain. Thus, in clinical practice there may be regions of the head where the error of registration is lower than the RMSE, as well as regions where the error is greater. In addition, strict comparison of RMSE values between navigation systems is only possible when similar registration methods, fiducial positions, and localization techniques are used.

The phantom tests of localization accuracy showed that the magnitude of error for frameless stereotaxy was at least comparable with that accompanying frame-based stereotaxy. In the landmark investigations of Maciunas and coworkers[20,21] the best application accuracy of the Cosman-Roberts-Wells system (Radionics, Inc.) was 1.8 mm with an SD of 1.1 mm, giving a 95% confidence limit (CL) of 3.6 mm. By comparison the error of phantom frameless stereotaxy for 2-mm CT slices was 1.1 mm with an SD of 0.5 mm, giving a 95% CL of 2.1 mm. The phantom frameless stereotaxy experiments described here also revealed that error with CT scanning was significantly lower than for procedures directed by MR imaging. This is in agreement with the findings for frame-based stereotaxy and reflects both the greater geometrical stability of CT scanning and the smaller voxel size. Similarly, 2-mm CT slices provided significantly more accurate guidance than 3-mm slices in frameless stereotaxy, and slice thickness has been shown to be the major determinant of error

TABLE 3

*Summary of in vivo accuracy assessment for frameless stereotactic biopsy in 13 patients**

Case No.	Preop Imaging	Postop Imaging	RMSE of Image Fusion (mm)	Linear Error (mm)				E Error (mm)
				X-Axis	Y-Axis	Z-Axis	Mean	
3	MR (S)	MR (S)	1.0	0.5	2.4	5.8	2.4	4.6
6	MR (S)	MR (S)	0.8	0.2	1.7	2.4	3.9	8.1
7	MR (S)	MR (S)	0.8	0.3	1.0	3.8	3.6	6.5
8	MR (S)	MR (S)	1.5	2.3	0.5	6.7	2.0	4.0
9	CT	MR (S)	1.8	2.2	5.1	2.3	2.5	6.1
10	CT	MR (V)	0.8	5.9	1.5	0.3	3.2	6.0
12	CT	MR (V)	0.5	0.7	0.2	0.9	2.9	6.3
	CT	MR (V)	0.5	1.8	1.8	0.2	1.4	3.0
13	MR (S)	MR (S)	1.3	0.0	1.8	0.3	0.7	1.8
14	CT	MR (S)	1.5	4.7	2.7	3.5	1.7	3.9
15	CT	MR (V)	2.4	0.8	3.6	1.6	3.1	7.1
16	MR (V)	MR (V)	0.4	0.3	5.3	6.1	0.6	1.2
17	MR (V)	MR (V)	0.7	1.4	3.9	2.0	1.2	2.6
19	MR (V)	MR (V)	0.5	5.6	3.9	2.0	2.9	5.2
	MR (V)	MR (V)	0.5	4.0	2.9	1.7	2.4	5.7

* E = Euclidean; MR (S) = Signa 1.5-tesla MR imager; MR (V) = Vectra 0.5-tesla MR imager.

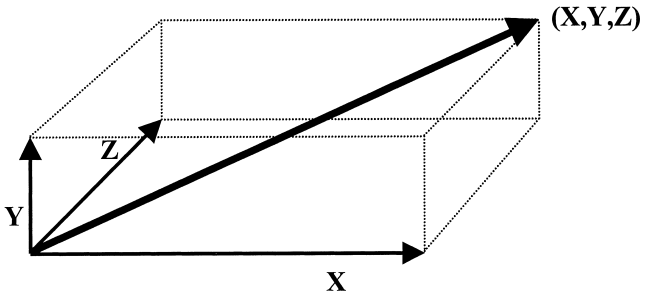

FIG. 6. Illustration emphasizing the relationship between linear (X, Y, or Z) and euclidean (X,Y,Z) errors. Note that the euclidean value is by definition much larger than any of the constituent linear values.

in CT-directed frame-based stereotaxy.[4,21] The finding that 3-mm helical CT scanning was significantly more accurate than 3-mm axial CT scanning reflects the use of a smaller FOV in the former studies, reducing voxel size. It is interesting to note that the mean error of phantom frameless stereotaxy closely followed the mean intervoxel distance for that imaging study, implying that the limiting factor to accuracy of frameless stereotaxy was voxel size.

The phantom measurements of MR image–directed frameless stereotactic localization revealed a mean error of 1.4 mm. Reports in the literature of comparable phantom accuracy measurements for MR image–directed frame-based stereotaxy reveal localization errors of up to 5 to 10 mm.[5,6,29] The superior accuracy of frameless MR image–directed stereotaxy may be explained through reductions in image distortions. Thus, registration with peripheral frame N fiducial markers is inherently less accurate than registration in which the more central skin-surface fiducial markers are used. In addition, the size of some MR imaging–compatible frames precludes the use of a head coil, frames themselves cause field distortions,[5,19] and frame geometry may be altered during the pin tightening.[16]

When early postoperative MR imaging studies were performed for the frameless stereotactic biopsy in vivo error study, the biopsy sites were found to be displayed with remarkable clarity. However, the same biopsy sites were not clearly visualized with CT scanning. This suggested that the low signal ellipsoid visible on MR imaging represented an area of tissue loss that was filled with cerebrospinal fluid or tissue fluid. Although we acknowledge that any brain shift, bleeding, or swelling would increase the measured errors of frameless biopsy, we accepted this ellipsoid as the site of biopsy with a high level of confidence. Subtraction of the coordinate values for the intraoperative target from those of the biopsy site provided linear x, y, and z measurements with a mean error of 2.3 mm. These linear values provide a valuable indication of the confidence with which a structure may be reached in clinical practice. Thus, using the frameless method, to avoid a nearby structure with 95% confidence when selecting a biopsy target from an axial image slice, the target must lie on average 4.3 mm distant (mean error + 2 SDs).

The measurements of error described here for the phantom laboratory series represent the actual distance from the needle tip to the intended target site. This distance represents a vector in space, with x, y, and z components. Each of these component errors was analyzed for a significantly elevated error, but none was discovered. Similarly, the linear in vivo errors were analyzed for each of the x, y, and z components, and no significant differences were detected. Although such linear error measurements enable these analyses and are applicable to single-slice stereotaxy, when three dimensions are involved, such as when the target is an anatomical structure in functional neurosurgery, the error measurements obtained should be converted to euclidean errors. These represent the vectorial distance between the target and the actual biopsy site in three-dimensional space and, ipso facto, are much greater than their constituent linear errors (Fig. 6).

The mean in vivo euclidean error for frameless stereotactic biopsy was found to be 4.8 mm, which represents an error volume of 0.46 cm^3 and a mean volume of 95% CL of 2.75 cm^3. Although some of these in vivo error results may appear large, there are no comparable in vivo results for frame-based surgery available, and several confounding factors inevitably have falsely elevated these measurements. Such factors include the incorporation of errors originating in the inexact pre- to postoperative image data set fusion method, postimaging brain distortion, and imaging errors. However, it is likely that similar results would be obtained should such a study be conducted for a frame-based system and these error values have clear clinical significance, requiring further detailed investigation. The mean in vivo errors associated with CT-directed frameless stereotactic biopsy were greater than those for MR image–directed procedures. Although this was not a statistically significant difference, this finding would concur with laboratory findings that accuracy closely followed voxel size, the CT scanning parameters used in the clinical study producing a larger MID than the MR imaging protocols (Table 1). The difference in the magnitude of the results for laboratory phantom studies and in vivo assessments is explicable by a variety of clinical factors not reproduced by the phantom series, including patient-induced field inhomogeneities, movement artifact, skin distortion, the additional error of image fusion, difficulty in accurately defining the biopsy site, and postimaging brain distortion.[9] Thus, it is likely that error is underestimated by phantom studies and overestimated by in vivo measurements.

The clinical series of frameless stereotactic biopsies demonstrated several of the advantages of this method over classic frame-based stereotactic techniques. First, imaging was performed in patients without induction of anesthesia, reducing scanning time, medical personnel requirements, and patient risk. Second, compared with frame-based biopsy procedures, operating room time was significantly reduced.[1] Third, the frameless method can be applied equally to the guidance of biopsy needles, biopsy forceps, ventricular catheters, depth electrodes, and endoscopes and may readily be adapted to guide additional instruments. Fourth, MR image–directed stereotaxy may be undertaken without MR imaging–compatible surgical equipment. Fifth, additional targets may be selected at any point during the procedure without further imaging. Sixth, surgical access to the skull is unimpeded and a burr-hole

procedure may be converted to an open operation without difficulty and with continued guidance. The clinical series also served to validate the frameless method of biopsy retrieval because all specimens could be diagnosed appropriately and no complications were encountered.

The movement check showed that the arm provided a robust platform for biopsy retrieval and, with reasonable care, did not move at all during the procedure. Furthermore, the system described here may equally be applied to other stereotactic procedures including functional neurosurgery. However, we would advocate the completion of a large series of stereotactically obtained biopsy specimens and further accuracy assessments before the introduction of functional operations. In addition, we would emphasize that the use of frameless stereotactic methods requires care and vigilance to ensure that excessive errors are not introduced. Although care is also required in frame-based stereotaxy, the errors are more uniform and predictable than those encountered with frameless systems, particularly with regard to registration. Thus, the clinician using a frameless system must have a clear understanding of the factors affecting registration and accuracy in neuronavigation. With this proviso, the studies described here suggest that frameless stereotaxy may be applied widely, safely, and advantageously in clinical practice, complementing the frame-based techniques and increasing the neurosurgical armamentarium.

Conclusions

The technique described here achieves true frameless stereotaxy. The method significantly reduces operation time, allows rapid interactive selection of multiple targets, dissociates image acquisition from surgery, and is compatible with all imaging modalities. Phantom investigations of accuracy have demonstrated the frameless technique to be at least as accurate as frame-based methods, and the frameless technique has been used to perform a series of clinical biopsy procedures with complete success. Furthermore, the magnitude of the in vivo error of stereotactically obtained biopsy specimens has been examined and estimates of confidence in clinical stereotaxy have been described.

Acknowledgments

This research and clinical validation work was performed within the context of the EASI project, "European Applications for Surgical Interventions," supported by the European Commission under contract HC1012 in their "4th Framework Telematics Applications for Health" research and technological development (RTD) program. The partners in the EASI consortium are The National Hospital for Neurology and Neurosurgery in London, Philips Medical Systems Nederland B.V., Philips Research Laboratory Hamburg, the Laboratory for Medical Imaging Research of the Katholieke Universiteit Leuven, the Image Sciences Institute of Utrecht University and University Hospital Utrecht, and the Image Processing Group of Radiological Sciences at the United Medical and Dental Schools of Guy's and St. Thomas' Hospitals in London.

References

1. Alberti O, Dorward NL, Kitchen ND, et al: Neuronavigation—impact on operating time. **Stereotact Funct Neurosurg 68:** 46–48, 1997
2. Barnett GH, Kormos DW, Steiner CP, et al: Use of a frameless, armless stereotactic wand for brain tumor localization with two-dimensional and three-dimensional neuroimaging. **Neurosurgery 33:**674–678, 1993
3. Barnett GH, Steiner CP, Weisenberger J: Target and trajectory guidance for interactive surgical navigation systems. **Stereotact Funct Neurosurg 66:**91–95, 1996
4. Bucholz RD, Ho HW, Rubin JP: Variables affecting the accuracy of stereotactic localization using computerized tomography. **J Neurosurg 79:**667–673, 1993
5. Burchiel KJ, Nguyen TT, Coombs BD, et al: MRI distortion and stereotactic neurosurgery using the Cosman-Roberts-Wells and Leksell frames. **Stereotact Funct Neurosurg 66:**123–136, 1996
6. Derosier C, Delegue G, Munier T, et al: IRM, distorsion géométrique de l'image et stéréotaxie. **J Radiol 72:**349–353, 1991
7. Dorward NL: Neuronavigation—the surgeon's sextant. **Br J Neurosurg 11:**101–103, 1997
8. Dorward NL, Alberti O, Dijkstra A, et al: Clinical introduction of an adjustable rigid instrument holder for frameless stereotactic interventions. **Comput Aided Surg 2:**180–185, 1997
9. Dorward NL, Alberti O, Velani B, et al: Postimaging brain distortion: magnitude, correlates, and impact on neuronavigation. **J Neurosurg 88:**656–662, 1998
10. Dorward NL, Wadley J, Alberti O, et al: One hundred consecutive cases with EasyGuide Neuro. **Comput Aided Surg 2:**209, 1997 (Abstract)
11. Drake JM, Rutka JT, Hoffman HJ: ISG Viewing Wand System. **Neurosurgery 34:**1094–1097, 1994
12. Fuchs M, Wischmann HA, Neumann A, et al: Accuracy analysis for image-guided neurosurgery using fiducial skin markers, 3D CT imaging, and an optical localizer system, in Lemke HU, Vannier MW, Inamura K, et al (eds): **CAR 96. Computer Assisted Radiology.** Amsterdam: Elsevier, 1996, pp 770–775
13. Golfinos JG, Fitzpatrick BC, Smith LR, et al: Clinical use of a frameless stereotactic arm: results of 325 cases. **J Neurosurg 83:**197–205, 1995
14. Gomez H, Barnett GH, Estes ML, et al: Stereotactic and computer-assisted neurosurgery at the Cleveland Clinic: review of 501 consecutive cases. **Cleveland Clin J Med 60:**399–410, 1993
15. Henderson JM, Eichholz KM, Bucholz RD: Decreased length of stay and hospital costs in patients undergoing image-guided craniotomies. **J Neurosurg 86:**367A, 1997 (Abstract)
16. Kamiryo T, Laws ER Jr: Stereotactic frame-based error in magnetic-resonance-guided stereotactic procedures: a method for measurement of error and standardization of technique. **Stereotact Funct Neurosurg 67:**198–209, 1996/97
17. Laborde G, Klimek L, Harders A, et al: Frameless stereotactic drainage of intracranial abscesses. **Surg Neurol 40:**16–21, 1993
18. Maciunas RJ, Berger MS, Copeland B, et al: A technique for interactive image-guided neurosurgical intervention in primary brain tumors. **Neurosurg Clin North Am 7:**245–266, 1996
19. Maciunas RJ, Fitzpatrick JM, Gadamsetty S, et al: A universal method for geometric correction of magnetic resonance images for stereotactic neurosurgery. **Stereotact Funct Neurosurg 66:** 137–140, 1996
20. Maciunas RJ, Galloway RL Jr, Latimer J, et al: An independent application accuracy evaluation of stereotactic frame systems. **Stereotact Funct Neurosurg 58:**103–107, 1992
21. Maciunas RJ, Galloway RL Jr, Latimer JW: The application accuracy of stereotactic frames. **Neurosurgery 35:**682–695, 1994
22. Maurer CRJ, Fitzpatrick JM, Wang MY, et al: Registration of head volume images using implantable fiducial markers. **IEEE Trans Med Imaging 16:**447–462, 1997

23. Roessler K, Ungersboeck K, Dietrich W, et al: Frameless stereotactic guided neurosurgery: clinical experience with an infrared based pointer device navigation system. **Acta Neurochir 139:**551–559, 1997
24. Rohling R, Munger P, Hollerbach JM, et al: Comparison of relative accuracy between a mechanical and an optical position tracker for image-guided neurosurgery. **J Image Guid Surg 1:** 30–34, 1995
25. Sandeman DR, Gill SS: The impact of interactive image guided surgery: the Bristol experience with the ISG/Elekta viewing wand. **Acta Neurochir Suppl 64:**54–58, 1995
26. Sipos EP, Tebo SA, Zinreich SJ, et al: *In vivo* accuracy testing and clinical experience with the ISG viewing wand. **Neurosurgery 39:**194–202, 1996
27. Smith KR, Frank KJ, Bucholz RD: The NeuroStation—a highly accurate, minimally invasive solution to frameless stereotactic neurosurgery. **Comput Med Imaging Graph 18:**247–256, 1994
28. Spetzger U, Laborde G, Gilsbach JM: Frameless neuronavigation in modern neurosurgery. **Minim Invasive Neurosurg 38:** 163–166, 1995
29. Walton L, Hampshire A, Forster DMC, et al: Stereotactic localization with magnetic resonance imaging: a phantom study to compare the accuracy obtained using two-dimensional and three-dimensional data acquisitions. **Neurosurgery 41:** 131–139, 1997

Manuscript received February 25, 1998.
Accepted in final form August 18, 1998.
This research was supported by a grant from the European Union as part of the European Applications in Surgical Interventions (EASI) project.

Address reprint requests to: Neil L. Dorward, F.R.C.S., University Department of Neurosurgery, National Hospital for Neurology and Neurosurgery, Queen Square, London WC1N 3BG, United Kingdom.